NISTIR 5661

Fracture Testing of Large-Scale Thin-Sheet Aluminum Alloy

Roland deWit
Richard J. Fields
Samuel R. Low III
Donald E. Harne
Tim Foecke

U.S. DEPARTMENT OF COMMERCE
Technology Administration
National Institute of Standards
and Technology
(Formerly National Bureau of Standards)
Metallurgy Division
Gaithersburg, MD 20899

Prepared for the
Federal Aviation Administration
U. S. Department of Transportation
Washington, D.C.

NIST

NISTIR 5661

Fracture Testing of Large-Scale Thin-Sheet Aluminum Alloy

Roland deWit
Richard J. Fields
Samuel R. Low III
Donald E. Harne
Tim Foecke

U.S. DEPARTMENT OF COMMERCE
Technology Administration
National Institute of Standards
and Technology
(Formerly National Bureau of Standards)
Metallurgy Division
Gaithersburg, MD 20899

Prepared for the
Federal Aviation Administration
U. S. Department of Transportation
Washington, D.C.

May 1995

Issued June 1995

U.S. DEPARTMENT OF COMMERCE
Ronald H. Brown, Secretary

TECHNOLOGY ADMINISTRATION
Mary L. Good, Under Secretary for Technology

NATIONAL INSTITUTE OF STANDARDS
AND TECHNOLOGY
Arati Prabhakar, Director

Administrative Information

This report constitutes the final report on the Interagency Agreement No. DTGFA03-92-Z-00018, Task Number 4, with the Federal Aviation Administration, U. S. Department of Transportation. The technical contact at the FAA for this research was Dr. Michael L. Basehore, Federal Aviation Administration, Structural Performance Technology, Aging Aircraft, FAA Technical Center, Atlantic City International Airport, NJ 08405, (609)485-6342.

ABSTRACT: A series of fracture tests on large-scale, pre-cracked, aluminum alloy panel was carried out to examine and to characterize the process by which cracks propagate and link up in this material. Extended grips and test fixtures were specially designed to enable the panel specimens to be loaded in tension in a 1780-kN-capacity universal testing machine. Ten panel specimens, each consisting of a single sheet of bare 2024-T3 aluminum alloy, approximately 4 m high, 2.3 m wide, and 1 mm thick, were fabricated with simulated through-cracks oriented horizontally at mid-height. Using existing information, a test matrix was set up to explore regions of failure controlled by fracture mechanics, with additional tests near the boundary between plastic collapse and fracture. In addition, a variety of multiple site damage (MSD) configurations were included to distinguish between various proposed linkage mechanisms. All tests but one used anti-buckling guides. Three specimens were fabricated with a single central crack, six others had multiple cracks on each side of the central crack, and one had a single crack but no anti-buckling guides. The results of each fracture event were recorded on various media: film, video, computer, magnetic tape, and occasionally optical microscopy. The video showed the crack tip with a load meter in the field of view, using motion picture film for one tip and super VHS video tape for the other. The computer recorded the output of the testing machine load cell, the stroke, and twelve strain gages at 1.5 second intervals. A wideband FM magnetic tape recorder was used to record data from the same sources. The data were analyzed by two different procedures, (1) the plastic zone model based on the residual strength diagram, and (2) the R-curve. The first three tests were used to determine the basic material properties, and these results were then used in the analysis of the subsequent tests with MSD cracks. There is fairly good agreement between measured values and results obtained from the models.

KEY WORDS: aluminum, crack, fracture mechanics, multiple site damage, plastic zone, R-curve, toughness

Introduction

The aging of the commercial air transport fleets around the world is of constant concern because of the loss of structural integrity through fatigue cracking. In one design approach for aircraft fuselages using semi-monocoque construction, circumferential rings or frames are intended to steer dangerous longitudinal cracks—if they appear—in the less threatening circumferential direction around the fuselage. However, in the case of aging aircraft in which damage, such as short fatigue cracks emanating from rivet holes, is present, cracks that start running longitudinally may continue to do so because the cracked rivet holes may provide a path of lesser resistance. Therefore the Federal Aviation Administration (FAA) Technical Center has initiated several research projects to investigate the structural integrity of the aging fleet. Some of these initiatives address the occurrence of multiple cracking that appears to be an attribute of aging aircraft. The terms "Widespread Fatigue Damage" (WFD) and "Multiple Site Damage" (MSD) are commonly used to describe a type of multiple cracking that degrades the damage tolerance capability of an aircraft structure. The damage tolerance degradation may lead to a reduction in residual strength below the design limit. Therefore, the capability to accurately calculate the residual strength of an aircraft structure containing several cracks is important in performing damage tolerance assessments.

Our research is intended to provide some of the information needed to better understand the crack propagation process and the mechanics of multiple crack linkup. In this work we were greatly aided by the advice of David Broek. Also a team from NASA Langley under leadership of James C. Newman assisted with additional measurements. The specialized facilities and capabilities at NIST were used to carry out a series of fracture tests on ten large-scale, 2286 mm wide, pre-cracked, aluminum alloy panels to examine and to characterize the process by which cracks propagate and link up in this material. The tests were sponsored by the FAA as part of it's National Aging Aircraft Research Program. The current tests were deemed necessary by the FAA because in previous work [1,2] only 508 mm wide flat panels were tested, while all other tests were performed on 2286 mm wide curved panels loaded by pressure, both with and without frames and tear straps. The results of these previous tests were predicted very well with an analytic plastic zone model, but showed that the main mode of failure was plastic collapse. In the current program the wide plates failed under conditions closer to fracture mechanics and R-curve behavior.

Using existing information obtained from the tests with smaller specimen, we set up a test matrix that explores regions of failure that are controlled by fracture mechanics, with additional tests near the boundary between plastic collapse and fracture. In addition, a variety of multiple site damage (MSD) configurations were included to distinguish between various proposed linkage mechanisms. All tests but one were performed with the use of anti-buckling guides. The one without anti-buckling guides was recommended by NASA Langley to help assess the effect of buckling.

Four specimens were fabricated with a single central crack and one of these had no anti-buckling guides. The other specimens had multiple cracks on each side of the central crack. The results of each fracture event were recorded on various media: film, video, computer, magnetic tape, and the NASA team occasionally also added optical microscopy. Using flat sheets without

stringers to stiffen the panels, these were uncomplicated tests aimed more at obtaining basic material properties than actually simulating fracture in an airplane fuselage. The material properties sought were the basic fracture properties and linkage criteria for the MSD cracks.

The data were analyzed by two different procedures, (1) the plastic zone model based on the residual strength diagram, and (2) the R-curve. The plastic zone model is an engineering approach that takes the plasticity at an advancing crack tip into account by using an effective fracture toughness, which is less than the true fracture toughness of the material. The basic concept is that the residual strength in the presence of MSD depends on the criterion that an MSD crack will be absorbed by the main crack when their two plastic zones meet, and the ligament then fails by collapse. It has been a very good predictor of the test results. The R-curve uses a more fundamental approach but requires more data collection and analysis. It accounts directly for the plasticity effects by the R-curve behavior of the material, and gives more detailed information of the fracture event, such as the amount of crack growth before instability.

The first three tests each contained a single crack and the collected data were used to determine the basic material properties, namely tentative values of the collapse strength and the effective fracture toughness for the residual strength diagram, and an analytic expression for the R-curve. These results were then used in the analysis of the subsequent tests with MSD cracks.

Description of Tests

Since this effort used 2286 mm (90 in) wide panels, some with multiple site damage (MSD), it was named the "90 MSD" program. A typical test panel is shown in Fig. 1. A cross-section of the panel is shown in Fig. 2, with definitions of the relevant dimensions. The test matrix is given in Table 1 and also illustrated in Fig. 3. The individual tests are labeled MSD-1, MSD-2, etc. The figure also shows the stresses (MPa units) at linkup and at failure for each panel.

The uncertainties are of type B. The uncertainties in the crack length measurements in Tables 1 and 2 and Fig. 3 were evaluated at 1 mm. The uncertainty in the displacement measurement in Table 2 was evaluated at 0.5 mm. The uncertainties in the load and stress measurements in Table 2 and Fig. 3 were evaluated at 0.5 percent.

A dozen panels were procured, each consisting of a single sheet of bare (not clad) 2024-T3 aluminum alloy, 3988 mm high, 2286 mm wide, and 1.016 mm thick. The specimens were fabricated with simulated through-cracks oriented horizontally at mid-height. The simulated cracks were saw cuts, ending with the sharpest jeweler's saw cuts available, having a final tip radius of 0.076 mm. The first three tests each had a single central crack. Subsequent tests also had multiple small cracks on each side of a larger central crack to simulate multiple site damage (MSD). Each MSD crack had a circular 5.6 mm diameter hole in its center to simulate a rivet hole, as shown schematically in Fig. 1.

A review of the literature suggested that the specimens tested in this program were the largest structural panels that have been tested in tension. The great size necessitated special design and testing considerations in order to introduce the test loads uniformly along the panel widths. A whiffle-tree approach was ruled out by the height limitations of the 1780-kN-capacity four-screw-powered universal testing machine (UTM) that was used. As it was, 76 mm had to be

cut from the specimens reducing their height to 3912 mm, and only 30 mm to 50 mm of the testing machine's stroke remained at specimen failure. The machine is one of the largest electro-mechanical testing machines in the world. In its unaltered state, with power screws in all four corners of the 1068 mm × 1524 mm testing table, loads to 448 kN can be applied up to 914 mm off-center, and up to full capacity at 152 mm off-center.

However, to accommodate the large panels, the heads of the testing machine were effectively enlarged with pairs of wide flange structural steel beams (W8×40), 2286 mm long, bolted together. The grips consisted of 2286 mm-long, thick-walled aluminum-alloy extrusions bolted to the steel beams. Each end of the panel specimens was fastened between the grips with forty-five 15.875 mm high-strength steel bolts, fully tightened. The length of the panel between the top and bottom rows of bolts was 3810 mm. Abrasive cloth was inserted between the specimens and the grips to maximize the transfer of load by shear and thereby avoid pin bearing failures of the thin panel material.

The uniformity with which the load was introduced was monitored in the first test with 20 strain gages and in subsequent tests with 10 strain gages, mounted on each panel about 406 mm from the grips at each end. These were called the far field strain gages. The strain distribution was measured at low loads, prior to each test, and, if necessary, thin metal shims were inserted between the steel beams and the grips in order to achieve a more uniform distribution. Uniformities within ±10 percent were obtained in all cases.

Anti-buckling guides, consisting of four aluminum channels, were used to restrain out-of-plane buckling of the panel. The beams were placed horizontally about 12 mm above and below the crack on both sides of the specimen. In the first test a 12 mm thick felt pad was used between the guides and the specimen to facilitate smooth sliding. In subsequent tests rubber was used. Test MSD-6 was performed without the anti-buckling guides to ascertain their effect.

The tests consisted of pulling the specimen to fracture under displacement control. The displacement was generally applied at load intervals of 20 to 45 kN and held for one to four minutes at each load level. The whole test lasted from 15 to 20 minutes. Link-ups to MSD cracks occurred in a fraction of a second. Towards the end of the test there was a large amount of crack growth with very small increase of load. After 50 to 100 mm of crack growth, tearing instability occurred and the load started to drop. Final fracture occurred with an audible rip.

Data Collection

The tests were highly instrumented and the data collection had some built-in redundancy for the sake of quality control and possible component failure. Besides the far field strain gages mentioned above, eight additional gages (twelve for the first test) were placed near the crack tips or MSD cracks. The strain gage signals were run through wide band strain gage conditioning amplifiers. A displacement gage was installed at the bottom of the cross head to measure the total displacement. For specimens MSD-4, 5 and 7 through 10 a clipgage was also mounted at the middle of the central crack. The signals of all these gages were recorded by a personal computer and a magnetic tape recorder. Since these signals were recorded as a voltage, prior to each test various calibration runs were performed to be able to convert these voltage readings later to the appropriate physical quantities. For MSD-2, 3, 4 and 6 a team from NASA Langley assisted with

the tests and also used high resolution optical microscopy. Test MSD-6, which had no anti-buckling guides, used thirteen three-element rosette strain gages. Seven of these were in the two crack paths and four were near the center of the crack. The data collection can be divided into five categories: manual, video, computer, magnetic tape, and optical microscopy.

Manual Recording

During the test at each load level the load was noted from the dial of the universal testing machine (UTM). The strain at these loads was read with a bridge amplifier at some of the far field gages near the top and bottom of the specimen. For tests MSD-1 and 7 all the far field strain gages were manually recorded and for MSD-6 none were manually recorded. These recordings provided a record of the average strain and its uniformity across the panel. When the final fracture occurred the fracture load was also recorded from the dial of the UTM.

Video Recording

A super VHS (SVHS) video camera was mounted to view the right crack tip and a motion picture camera viewed the left during each test. The video recording consisted of showing a voltmeter with a crack tip and the MSD cracks (when present) in the field of view. The two voltmeters were connected to the UTM load cell and showed a voltage proportional to the load. A calibration was run for the voltmeters prior to the test. The SVHS recording could be observed on a TV screen during recording; thus, the progress of the crack growth could be monitored. After the test the video recordings were used to determine the crack extension as a function of the load.

Computer Recording

A personal computer was used to collect and store data from various sources. These data included the current time, the load obtained from the UTM load cell, the displacement, the strains from the far field gages that were not taken manually, the gages near the crack, and for tests MSD-4, 5, and 7 to 10 the clipgage. Each data set was taken at 1½ second intervals, was shown on the video monitor, and stored in a file.

As mentioned the input data were read as a voltage. Therefore, calibrations were run prior to each test. For the load calibration a simulated load was generated at the UTM console with 22.2 kN intervals from zero up to 200 or 450 kN. The displacement gage was calibrated at 0.254 and 0.635 mm intervals over a range of 20 mm. The strain gages had a resistance of 350 Ω and a gage factor of 2.135. They were calibrated using the strain gage conditioning amplifiers, which also contained bridge resistances of 350 Ω. With a switch, a shunt resistance of 174.8 kΩ could be shorted across the bridge, which corresponded to a simulated strain change of 936 microstrain. The above calibrations resulted in linear conversions. The clipgage worked on the capacitive principle and was calibrated at 0.635 mm intervals from zero to 15 mm. It resulted in a nonlinear conversion of the form $a+bx+cx^2\sqrt{x}+d/x$.

Tape Recording

A wideband FM magnetic tape recorder was used to record data from the same sources as the computer recording. The tape recorder was set to IRIG I and run at 30 inch per second, which provides a distortion free signal (1 dB) from DC to 20 kHz. These recordings are fast enough to show dynamic effects. These data have not yet been analyzed.

Optical Microscopy (OM)

For tests MSD-2, 3, 4 and 6 a team from NASA Langley collaborated with high resolution optical microscopy (OM) at one crack tip. For test MSD-6 they additionally recorded the signals from the 3-element rosette strain gages. Their optical microscopy apparatus was used to observe the growing crack. A photographic technique was developed to measure the crack tip opening angle during crack initiation and stable tearing. The OM apparatus consisted of a computer controlled, long focal length microscope fitted to a video camera. The field of view of the microscope was a square with sides approximately 1.8 mm long. The field of view was centered on the crack tip and advanced as the crack grew. The results from this analysis will be reported elsewhere by NASA Langley.

at the left crack tip from the backside.

R-Curve Analysis

The crack extension that occurred as the load increased was measured with the SVHS video tape, the movie film, and the OM apparatus. The results for tests MSD-1, 2, 3 and 6 are shown in Fig. 4. These tests all had a single central crack, see Table 1. Specimen MSD-6 had no anti-buckling guides and the data for this test fall below those for MSD-3, which had the same crack size. This result shows that the lack of guides and consequent buckling acted as a stress intensification at the crack tips.

We have used the R-curve concept [3] to analyze some of the data. First, we show how to find the crack-extension force, G, from the crack growth data. This quantity is related to the stress-intensity factor, K, by

$$G = \frac{K^2}{E} \tag{1}$$

where E is Young's modulus. The stress-intensity factor is generally given by the generic expression

$$K = \beta\sigma\sqrt{\pi a} \tag{2}$$

where the function β is used to describe the effect of the shape and size of the crack and the specimen. For the center crack specimen we then have

$$G(a) = \frac{\sigma^2 \pi a}{E} \beta^2\left(\frac{\pi a}{W}\right) \tag{3}$$

where σ is the applied stress, a the half-crack size, and W the panel width. For the stress-intensity factor of a center-notch specimen with sharp crack tips Feddersen [4] discovered that

$$\beta\left(\frac{\pi a}{W}\right)=\sqrt{\sec\left(\frac{\pi a}{W}\right)} \tag{4}$$

gives an approximation that is accurate to 0.3 percent for $2a/W < 0.7$. The applied stress is given by

$$\sigma=\frac{P}{WB} \tag{5}$$

where P is the load and B is the panel thickness. In our experiments:

$$W = 228 \text{ mm}$$

$$B = 1.016 \text{ mm}$$

$$E = 71 \text{ GPa}$$

Using these values and Equations (3)-(5), the movie film and video tape data from Fig. 4 were converted into the crack-extension force data shown in Fig. 5. We see that for small crack-extensions the data from the tests with the anti-buckling guides collapse nicely into a master curve, but without anti-buckling guides the data are distinctly different. Now, according to the R-curve concept the crack-extension resistance, R, equals the crack-extension force, G, for slow stable crack growth with a sharp crack tip. We wish to identify those points for tests MSD-1, 2, and 3 (shown solid in Fig. 5) that qualify as R-curve data. The data with no crack-extension represent the original blunt notch and so do not yet represent crack growth along the R-curve. For short crack-extensions up to about 75 mm there is slow stable crack growth, while for larger crack-extensions there is unstable dynamic crack growth. Initially, we did not know the critical point of instability that separated the stable from the unstable data for each test. We, therefore, used an iterative procedure and started with an initial estimate for the critical crack-extension. To represent the R data by a universal R-curve, a power law was fitted to the data, giving

$$R = 75.9da^{0.28} \tag{6}$$

where R is measured in kN/m and da in mm. With an analytic expression for the R-curve the point of instability can be found. The stability diagram in Fig. 6 illustrates this for test MSD-1. A crack-extension force line or G-line is drawn and the control parameter is adjusted until the line is tangent to the R-curve when it becomes the G_c-line. For simplicity we can take for G the expression for the infinite plate with a single crack ($\beta = 1$) under load or stress control

$$G=\frac{\sigma^2\pi a}{E} \tag{7}$$

because for cracks under 500 mm in the test panels this equation does not differ much from the correct expression below (Equation 11). Equation (7) gives a straight line in Fig. 6. Tangency is achieved by adjusting the stress until a critical value of $\sigma_c = 146$ MPa is obtained, which then gives a critical crack-extension of $da_c = 69.3$ mm and a critical crack-extension force of $G_c = 248$

kN/m. Hence, the data points for which $0 < da < 69.3$ mm are stable for MSD-1 and those points were used for the curve fit in Fig. 5. The same procedure was applied to the data of tests MSD-2 and 3. If the initial estimate for da_c was wrong the procedure was repeated until all the fitted points lie below the points of tangency. Fig. 6 shows that for $da > da_c$ the unstable points lie closer to the G_c-line than the R-curve.

The testing machine was operated under displacement control so that the displacement, δ, is the control parameter. This quantity is related to the stress by

$$\sigma = \frac{\delta}{BWC_t} \tag{8}$$

where C_t is the total compliance of the testing system, which can be decomposed into the machine, panel, and crack compliance, as follows

$$C_t = C_m + \frac{H}{EBW} + \frac{4}{\pi EB} I\left(\frac{\pi a}{W}\right) \tag{9}$$

where H (3810 mm = 150 in) is the panel height and the function I is given by

$$I(x) = \int x\beta(x)\,dx \tag{10}$$

The total compliance was found for each test from the slope of the measured total displacement versus load curve. Using the slope before any crack extension occurred, Equation (9) was used to deduce the machine compliance. The average for the first three tests was $C_m = 1.082 \times 10^{-5}$ m/kN (± 4%). The complete expression for the G-line under displacement control is then given by combining Equations (3), (8), and (9) into

$$G(a) = \frac{E\delta^2 \pi a \beta^2\left(\frac{\pi a}{W}\right)}{\left[EBC_m + H + \frac{4W}{\pi} I\left(\frac{\pi a}{W}\right)\right]} \tag{11}$$

To find the critical point of instability, as was done in Fig. 6, the displacement is adjusted in this equation until tangency to the R-curve is achieved. In this way critical values are found for the displacement, δ_c, crack-extension, da_c, and crack-extension force, G_c. The critical stress, σ_c, is found by Equation (8) or (3), the fracture load, P_c, by Equation (5), and the toughness, K_c, by Equation (1). The results for the first three tests are summarized in Table 2. This table also includes measured values and results from the residual strength diagram discussed in the next section. The agreement between the measured and predicted data points is illustrated in Fig. 7.

Residual Strength Diagram

The residual strength diagram is used in an engineering approach to determine how the residual strength of a structure depends on the crack geometry and the specimen size. It is shown schematically for a center cracked sheet structure in Fig. 8. The dotted line represents the residual strength of the panel assuming linear elastic fracture mechanics for an infinite sheet. The

straight line shows the residual strength assuming net section collapse of a sheet of width W. For small and large crack sizes, where these two curves intersect, there is a region of transition from one failure mode to the other. Feddersen [5] argued that two linear tangents to the idealized K curve can be used to establish a smooth and continuous curve for the residual strength. One tangent to the K curve is drawn from the point $\sigma = \sigma_Y$, where σ_Y is the stress at which the structure without crack collapses by plastic yielding. The other tangent is drawn from the point $2a = W$ that represents the width of the structure. The fracture toughness is customarily determined from the crack size at the failure stress by Equation (2). In Fig. 8 the simplest version of this equation is used with $\beta = 1$. However, in thin sheets where a significant amount of crack extension occurs before failure, the final crack size is generally not known. Therefore, the data points plotted in the residual strength diagram usually are the initial crack size and the final failure stress, i.e. the crack extension and plasticity are ignored in this model. To compensate for this inconsistency, an effective value of the toughness, denoted by K_e, is used which is lower than the true toughness, such as that obtained by the R-curve. A slight improvement to the analysis can also be made by taking the finite width of the panel into account ($\beta \neq 1$). So the fracture event can be characterized by the expression

$$K_e = \sigma_c \sqrt{\pi a_i \sec\left(\frac{\pi a_i}{W}\right)} \tag{12}$$

In this way a value of K_e = 111 MPa$\sqrt{m}$ was obtained as the average of the first three tests. As discussed in the previous section, the final crack size was also determined in these tests. So the fracture event can also be characterized by the expression

$$K_c = \sigma_c \sqrt{\pi a_c \sec\left(\frac{\pi a_c}{W}\right)} \tag{13}$$

In this way a value of K_c = 132 Mpa$\sqrt{m}$ was obtained. In the analysis of the residual strength diagram equation (12) is used to obtain the fracture stress and then equation (13) is used to obtain the final crack size. The results for the first three tests are given in Table 2. Fig. 9 illustrates the results; the predicted fracture points and paths are shown and the measured data points are plotted as solid squares. The results for all three tests are seen to fall in the fracture mechanics region of the diagram. There is good agreement between the measured data and the predictions for these single crack specimens.

The Link-Up Criterion

For the panels with multiple site damage (MSD) we have used the analysis of Broek [1]. Here we have a situation where small cracks exist ahead of the large central crack. The first link-up is governed by the stress-intensity factor of the combination of the main crack and the first MSD crack. The geometry factors of the two cracks must therefore be compounded by the effect of crack interaction. As the ligament undoubtedly will fail by plastic collapse or net section yield, the compounded stress intensity factor can be used to calculate the plastic zone of both cracks and used with the criterion that link-up occurs when the two plastic zones meet. Broek found that the best estimate of the plastic zone size for this application was given by the Irwin expression

$$r_p = \frac{1}{2\pi}\left(\frac{K}{\sigma_Y}\right) \tag{14}$$

where σ_Y is the collapse strength. This expression represents the plastic zone at the tip of the main crack and a similar expression holds for the plastic zone at the MSD crack. Here the stress-intensity factor is still given by Equation (2), but with the MSD crack nearby the function β that takes the crack interaction into account is much more complicated than Equation (4). To model the first link-up, Broek assumed that the main interaction was between one tip of the central crack and the first MSD crack in front of it, ignoring all the other MSD cracks. Thus, β will depend on the central crack size, a, the MSD crack size, a_{MSD}, and the ligament L between them (Fig. 2), so that Equation (2) becomes

$$K = \beta(a, a_{MSD}, L)\sigma\sqrt{\pi a} \tag{15}$$

A similar expression holds for the stress-intensity factor to use in the plastic zone at the MSD crack. For these β functions, Broek has derived approximations based on published expressions for the stress intensity factors of two unequal length collinear cracks, which we have used. The link-up criterion between the central and first MSD crack then is that the plastic zones meet, or

$$r_p + r_{pMSD} = L \tag{16}$$

or, from Equations (14) and (15)

$$\sigma = \sigma_Y \sqrt{\frac{2L}{a\beta^2 + a_{MSD}\beta_{MSD}^2}} \tag{17}$$

For test MSD-4 this expression is plotted as the first dashed curve in Fig. 10. Though it is not shown explicitly in Equation (17) this curve represents the final failure stress as a function of initial crack size, in the same sense as was discussed for Equation (12). The horizontal axis in Fig. 10 represents the central crack size, a. For the curves that are plotted the MSD crack size, a_{MSD}, and the position of the MSD crack, δ_{MSD}, are kept constant. However, as may be clear from Fig. 2, the ligament L then varies with a. For the central crack with size a = 177.8 mm, Equation (17) predicts the first link-up at σ = 81 MPa. This is shown by the intersection of the fracture path line with the first dashed curve in Fig. 10. After the first link-up the central crack has absorbed the first MSD crack and it is assumed that we now have a larger central crack, a = 195.58 mm, that interacts with the second MSD crack. Equation (17) is again used with these new parameters and plotted as the second dashed curve in Fig. 10. The predicted stress for the second link-up then is σ = 117 MPa. This procedure is then repeated for the third link-up and we find σ = 111 MPa at a = 220.98 mm. Since this stress is lower than for the second link-up, we conclude that the panel is super-critical and the fracture will run straight through after absorbing the second MSD crack at 117 MPa, as shown by the fracture path in Fig. 10. When all three MSD cracks have been absorbed by the central crack, it behaves as a large single crack of size a = 246.38 mm in the panel. Failure is then predicted by the simpler Equation (12), as also shown in Fig. 10. The results of this analysis for tests MSD-4, 5, and 7 through 10 are summarized in Table 3 and compared with the measured values.

R-Curve and MSD

We now apply the R-curve to the failure prediction of a panel with MSD cracks. We assume that an R-curve originates from each MSD crack as well as the main central crack, as shown by the solid lines in Fig. 11. Each R-curve is given by Equation (6). We then draw G_c-lines tangent to each R-curve to determine the link-ups and final instability. The G-lines are still given by an expression similar to Equation (3), but now the β function for the central crack must also take the interaction with the MSD crack into account

$$G(a) = \frac{\sigma^2 \pi a}{E} \beta^2(a, a_{MSD}, L) \tag{18}$$

For a given stress this equation gives the G-line under load control. Using the appropriate parameters for each MSD, the stress was then adjusted until tangency was achieved for each of the R-curves, as shown by the dashed lines in Fig. 11. The final fracture at 246.3 mm uses the same procedure as discussed before. With the MSD cracks the G-lines have quite a bit of curvature just before the instability point. The link-up stress for the third MSD crack is less than for the second. This indicates that, after link-up of the second MSD crack, the panel is super-critical and the fracture will run straight through after absorbing the second MSD crack. So we reach the same conclusion from this R-curve analysis as from the residual strength diagram analysis in the previous section.

The results for tests MSD-4, 5, and 7 through 10 are summarized in Table 3. There is fair agreement with the measured values and also with the results predicted from the plastic zone model. The residual standard deviation of both the errors for the RSD and the R-curve is 17 percent. Some of the qualitative discrepancies are as follows. For MSD-5 and 7 the prediction from both the R-curve and the plastic zone model is that the final fracture will occur together with the second and third link-up, whereas actually the stress had to be raised from 161 to 174 MPa for MSD-5 and from 88 to 92 MPa for MSD-7 after the second and third link-ups to achieve the final fracture. For MSD-8 no second link-up was predicted whereas in fact there was one.

Conclusion

Analysis appears to provide fairly good predictions of the residual strength, link-ups, and fracture of panels with multiple site damage (MSD) of different size and spacing. The critical fracture stress can be predicted by using either the plastic zone criterion or the R-curve analysis, and the results are virtually the same. Several improvements to the analysis can be made. Notwithstanding the large widths of the panels, the MSD cracks are quite small and closely spaced so that small discrepancies in these dimensions may affect the results. The values listed in Table 1 are nominal rather than accurate and could differ by as much as 2 mm. Therefore, more accurate measurements of the MSD configurations made under a microscope could improve the results. The plastic zone analysis uses estimates for the effective fracture toughness, K_e, and the collapse strength, s_Y. The values of these two quantities can be optimized by taking the results of all the tests into account. In the R-curve analysis load control was used and the backward growth of the MSD crack was ignored. Improvements in this analysis is complex, but possible. Displacement control would allow the load to drop in the analysis as in fact it did in all the MSD tests after the link-ups.

Acknowledgment

We wish to acknowledge the recommendations and participation of David Broek from FractuREsearch and also the support, guidance, and advice of Dr. Michael L. Basehore from the FAA Technical Center, Structural Performance Technology, Aging Aircraft. The work was supported under Interagency Agreement No. DTGFA03-92-Z-00018, Task Number 4, with the Federal Aviation Administration, U. S. Department of Transportation.

References

[1] Broek, D., "The Effects of Multi-Site-Damage on the Arrest Capability of Aircraft Fuselage Structures," FractuREsearch TR 9302, June 1993.

[2] Broek, D., Jeong, D. Y., and Thomson, D., "Testing and Analysis of Flat and Curved Panels with Multiple Cracks," FAA/NASA International Symposium on Advanced Structural Integrity Methods for Airframe Durability and Damage Tolerance, Charles E. Harris, Ed., NASA Conference Publication 3274, National Aeronautics and Space Administration, Hampton, VA, September 1994, pp. 85-98.

[3] Broek, D.: Elementary Engineering Fracture Mechanics, Martinus Nijhoff Publishers, 1987

[4] Feddersen, C. E.: "Discussion," Plane Strain Crack Toughness Testing of High Strength Metallic Materials, ASTM STP 410, by William F. Brown, Jr., and John E. Srawley, American Society for Testing and Materials, Philadelphia, 1966, p. 77

[5] Feddersen, C. E.: "Evaluation and prediction of the residual strength of center cracked tension panels," ASTM STP 486, American Society for Testing and Materials, Philadelphia, 1971, pp. 50-78

Table 1--Test Matrix for 90 MSD Program

Test No	Main crack		MSD cracks				Date of test
	2a (mm)	a (mm)	d_{MSD} (mm)	s_{MSD} (mm)	$2a_{MSD}$ (mm)	number per side	
MSD-1	355.6	177.8					7/23/93
MSD-2	203.2	101.6					8/25/93
MSD-3	508.0	254.0					9/13/93
MSD-4	355.6	177.8	190.5	25.4	10.16	3	11/29/93
MSD-5	142.24	71.12	88.9	38.1	15.24	3	12/1/93
MSD-6[a]	508.0	254.0	no anti-buckling guides				4/12/94
MSD-7	508.0	254.0	266.7	38.1	12.7	5	4/20/94
MSD-8	482.6	241.3	266.7	38.1	12.7	10	5/26/94
MSD-9	254.0	127.0	165.1	25.4	10.16	10	6/29/94
MSD-10[b]	508.0	254.0	266.7	38.1	12.7	5	7/1/94

[a] Recommended by NASA Langley
[b] Repeat of MSD-7

Table 2--Measured Data and Failure Predictions for the First Three 90 MSD Tests

		Half-Crack Size					
Test No Date		Initial (mm)	Final (mm)	Extension (mm)	Load (kN)	Stress (MPa)	Displacement (mm)
MSD-1 7/23/93	Measured	177.8			343	147	12.6
	RSD		244.3	66.5	339	146	
	R-curve		247.1	69.3	339	146	11.9
MSD-2 8/25/93	Measured	101.6			428	184	16.1
	RSD		142.0	40.4	455	196	
	R-curve		141.0	39.4	424	183	14.5
MSD-3 9/13/93	Measured	254.0			289	124	12.2
	RSD		340.4	86.4	280	121	
	R-curve		353.1	99.1	290	125	10.5

Table 3--Test Data and Analytical Predictions of Link-up and Final Fracture from the Residual Strength Diagram and the R-curves for the Tests with MSD Cracks

Test No Date	Event	Measured	RSD		R-curve	
		Stress (MPa)	Stress (MPa)	Error	Stress (MPa)	Error
MSD-4 11/29/93	1st Linkup	84	81	-4%	103	21%
	2nd Linkup	98	117	18%	118	19%
	Fracture	132	123	-8%	126	-5%
MSD-5 12/1/93	1st Linkup	138	136	-2%	163	17%
	2nd Linkup	161	185	14%	171	6%
	Fracture	174	(148)	-16%	148	-16%
MSD-7 4/20/94	1st Linkup	57	58	2%	79	33%
	2nd Linkup	88	116	27%	110	22%
	Fracture	92	(88)	-5%	92	-1%
MSD-8 5/26/94	1st Linkup	89	118	28%	110	21%
	2nd Linkup	91	(116)	24%	110	19%
	Fracture	73	(65)	-12%	67	-9%
MSD-9 6/29/94	1st Linkup	152	174	14%	165	8%
	2nd Linkup	(152)	(125)	-19%	(126)	-18%
	Fracture	119	(92)	-26%	97	-21%
MSD-10 7/1/94	1st Linkup	66	58	-13%	79	17%
	2nd Linkup	95	116	20%	110	14%
	Fracture	100	(88)	-13%	92	-9%

The numbers in parentheses are lower than for a previous link-up, thus failure will precede the link-up.

Figure Captions

Fig. 1--Typical 90 MSD test panel

Fig. 2--Cross-section of test panel with definitions of 90 MSD crack configurations and dimensions

Fig. 3--Test Matrix for 90 MSD Program. Stresses at linkup and failure are shown in units of MPa.

Fig. 4--Crack growth measurements for tests 90 MSD-1, 2, 3, and 6

Fig. 5--Crack-extension force data and analytic R-curve for tests 90 MSD-1, 2, 3, and 6

Fig. 6--Stability diagram for test 90 MSD-1

Fig. 7--Test data and analytical predictions from R-curve for tests 90 MSD-1, 2, and 3

Fig. 8--Residual strength diagram with analysis of Feddersen

Fig. 9--Residual strength diagram for tests 90 MSD-1, 2, and 3, with measured data points and predicted fracture paths

Fig. 10--Residual strength diagram for test MSD-4, with plastic zone criteria and predicted fracture path

Fig. 11--Stability diagram for test 90 MSD-4

Figure 1. Typical 90 MSD test panel

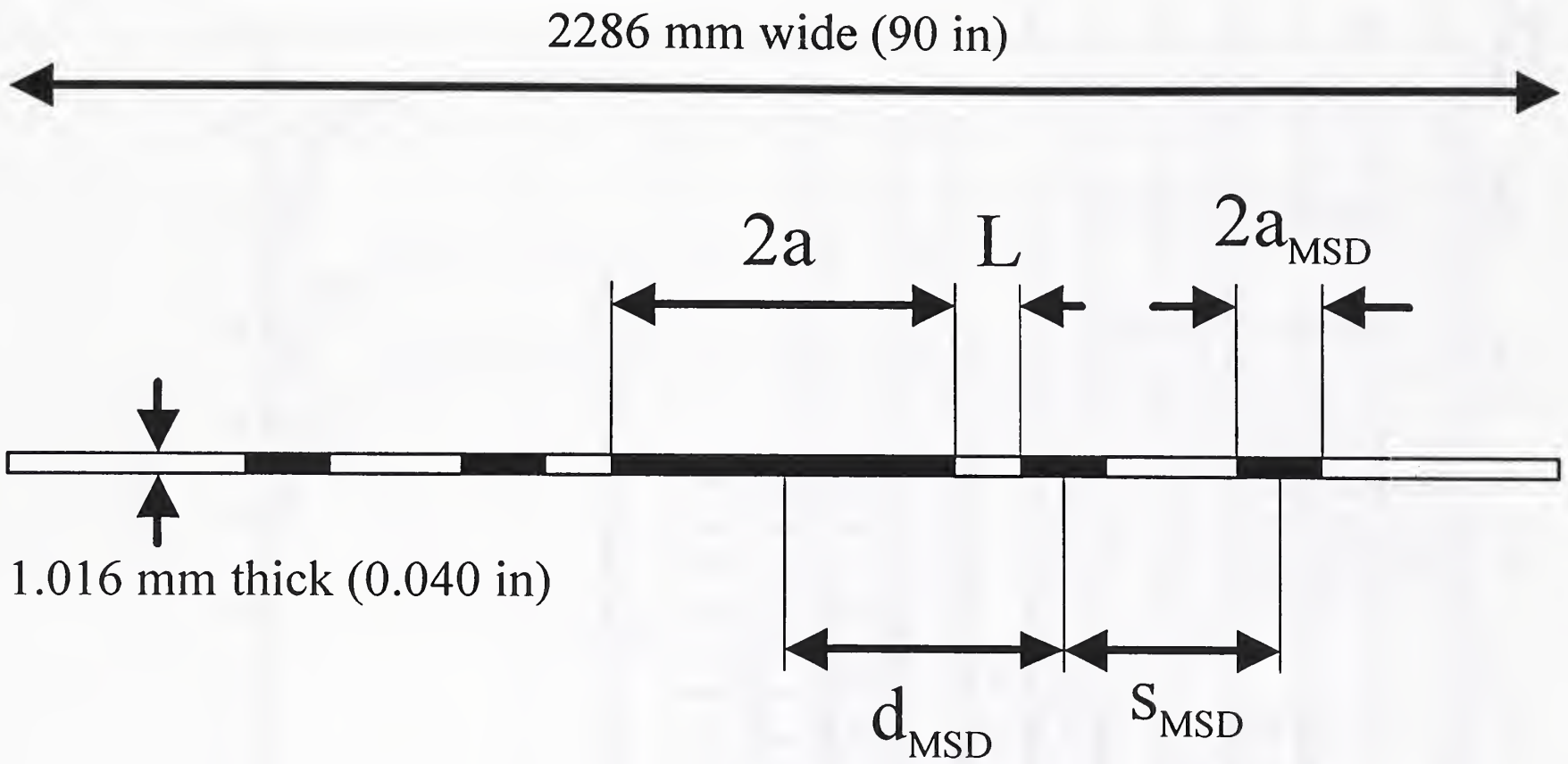

Figure 2. Cross-section of test panel with definitions of 90 MSD crack configurations and dimensions

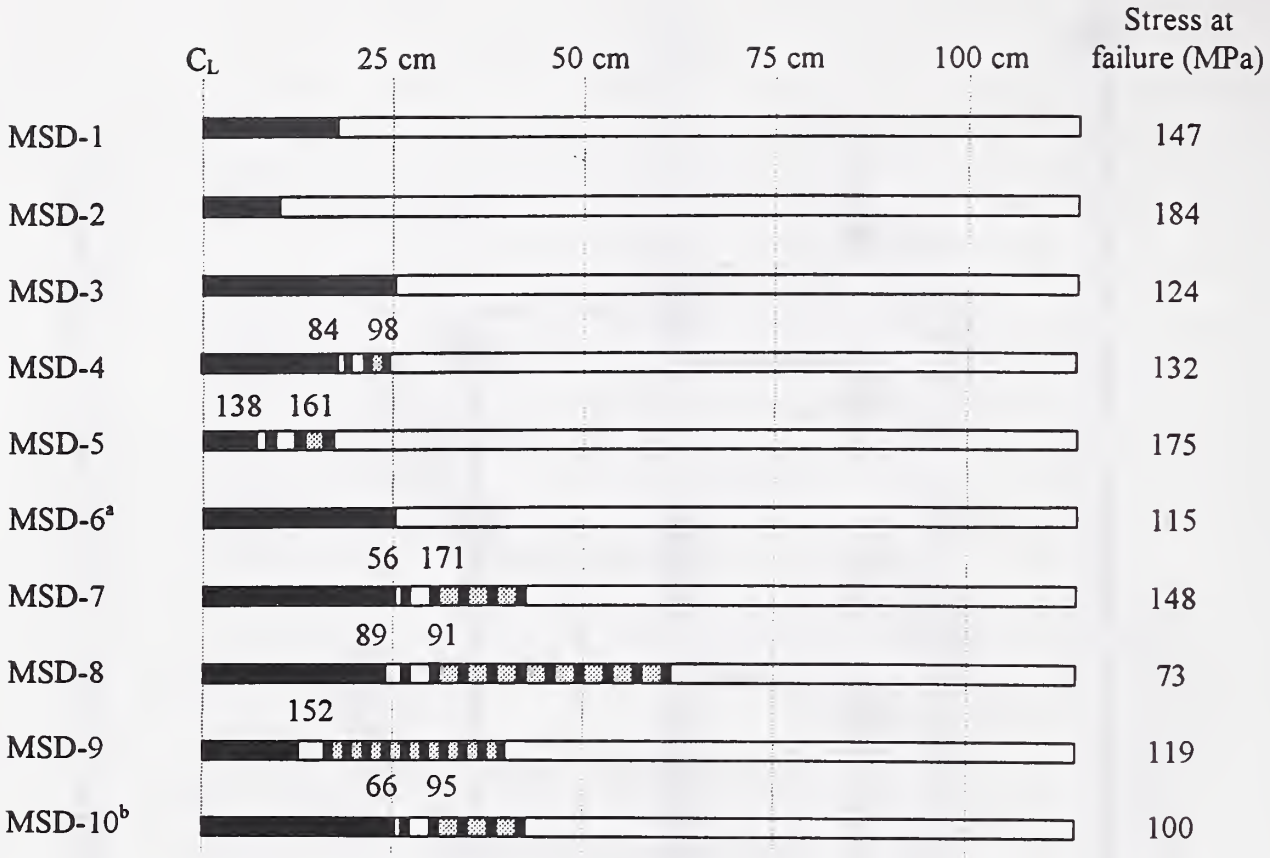

▨ Ligaments that failed simultaneously
[a] No anti-buckling guides
[b] Repeat of MSD-7

Figure 3. Test Matrix for 90 MSD Program

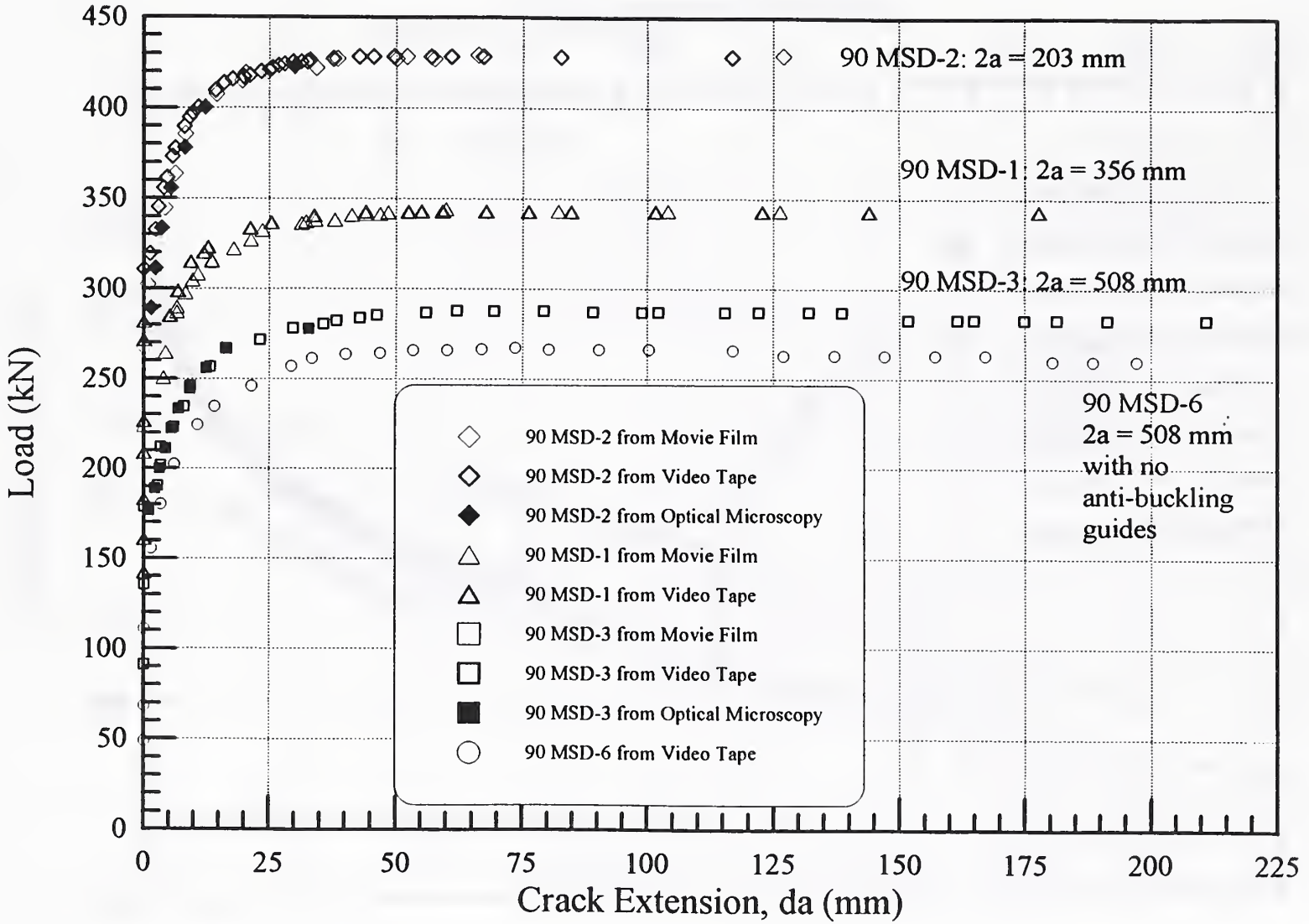

Figure 4. Crack growth measurements for tests 90 MSD-1, 2, 3 and 6

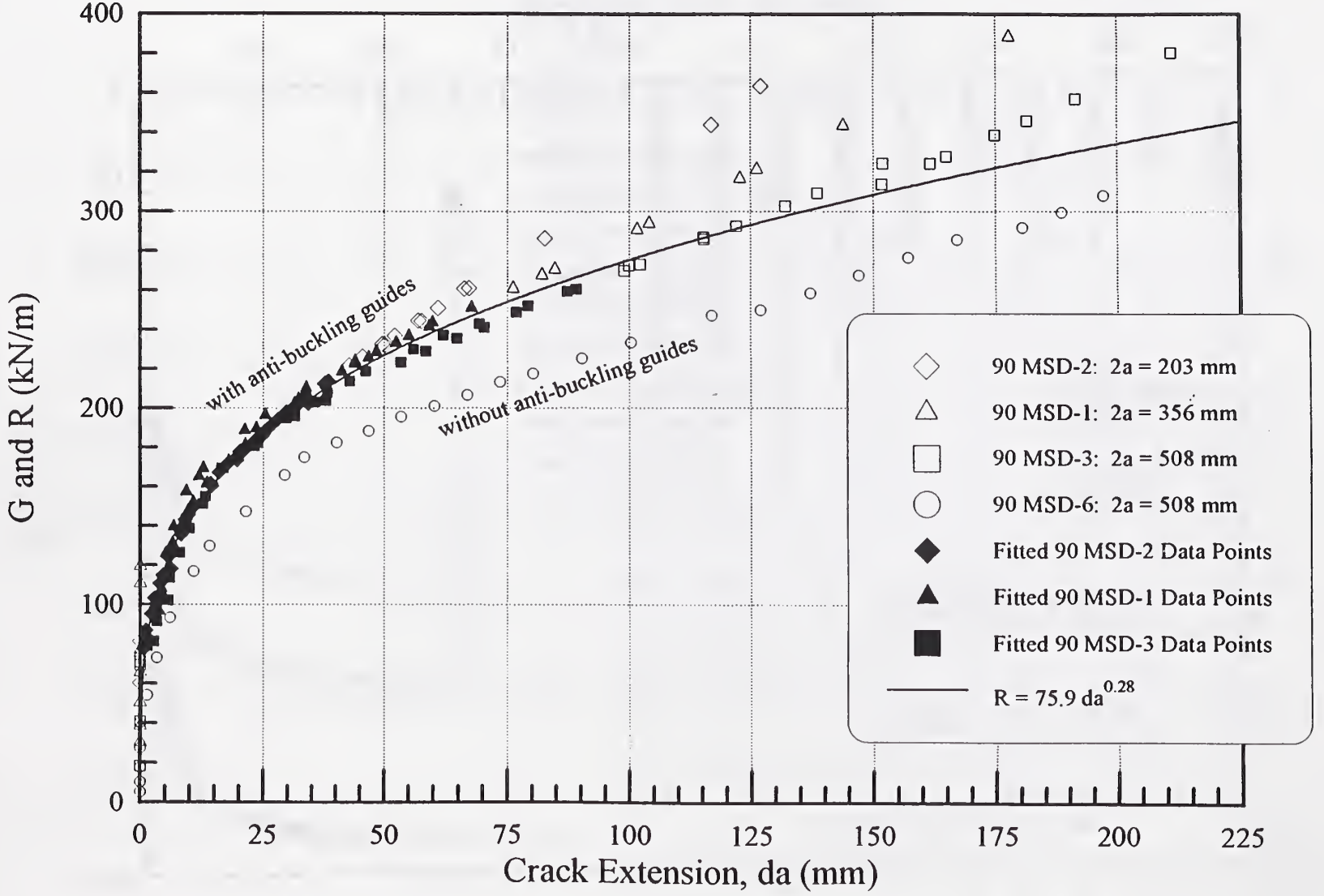

Figure 5. Crack-extension force data and analytic R-curve for tests 90 MSD-1, 2, 3 and 6

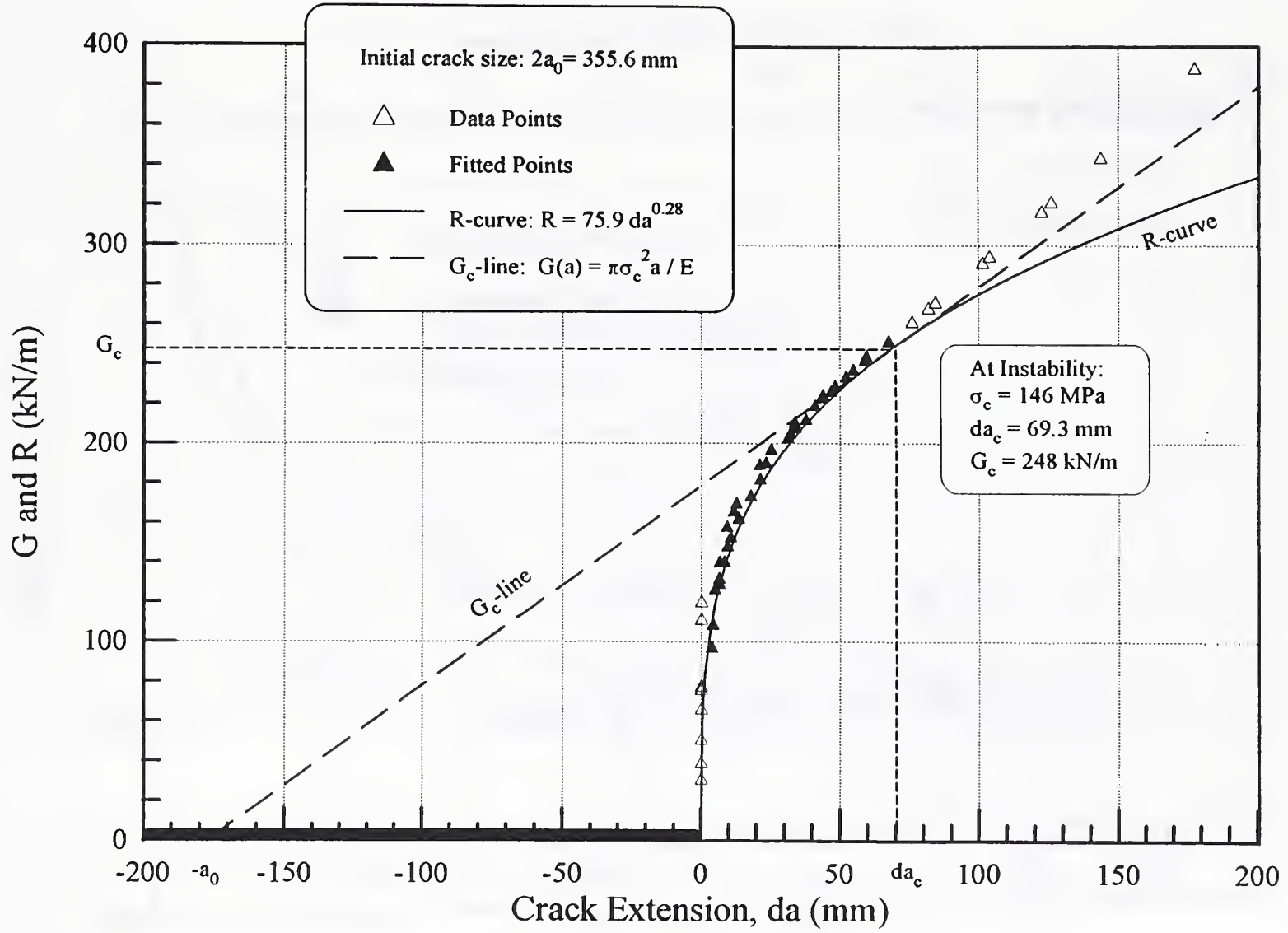

Figure 6. Stability diagram for test 90 MSD-1

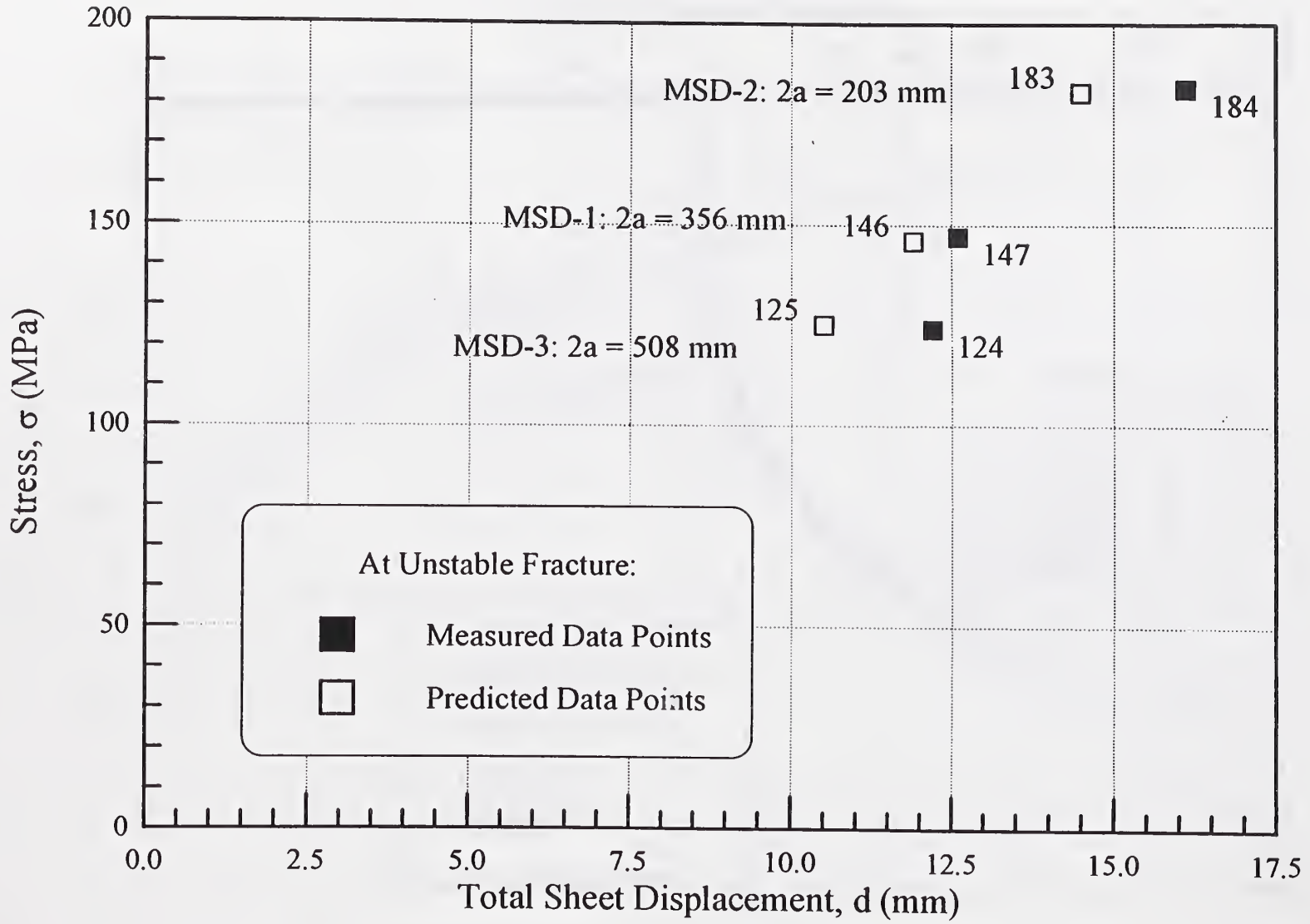

Figure 7. Test data and analytical predictions from R-curve for tests 90 MSD-1, 2, and 3

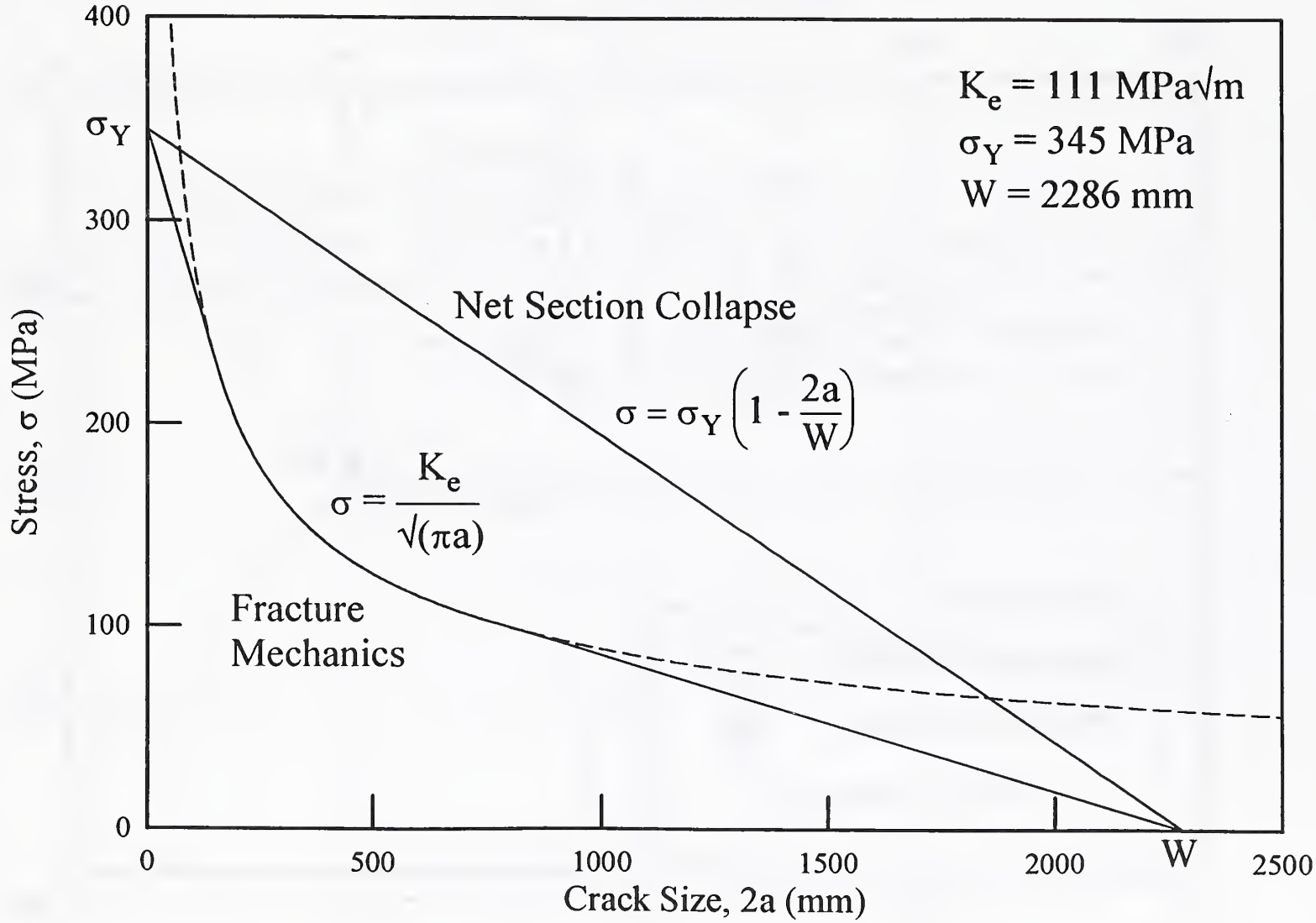

Figure 8. Residual strength diagram with analysis of Feddersen

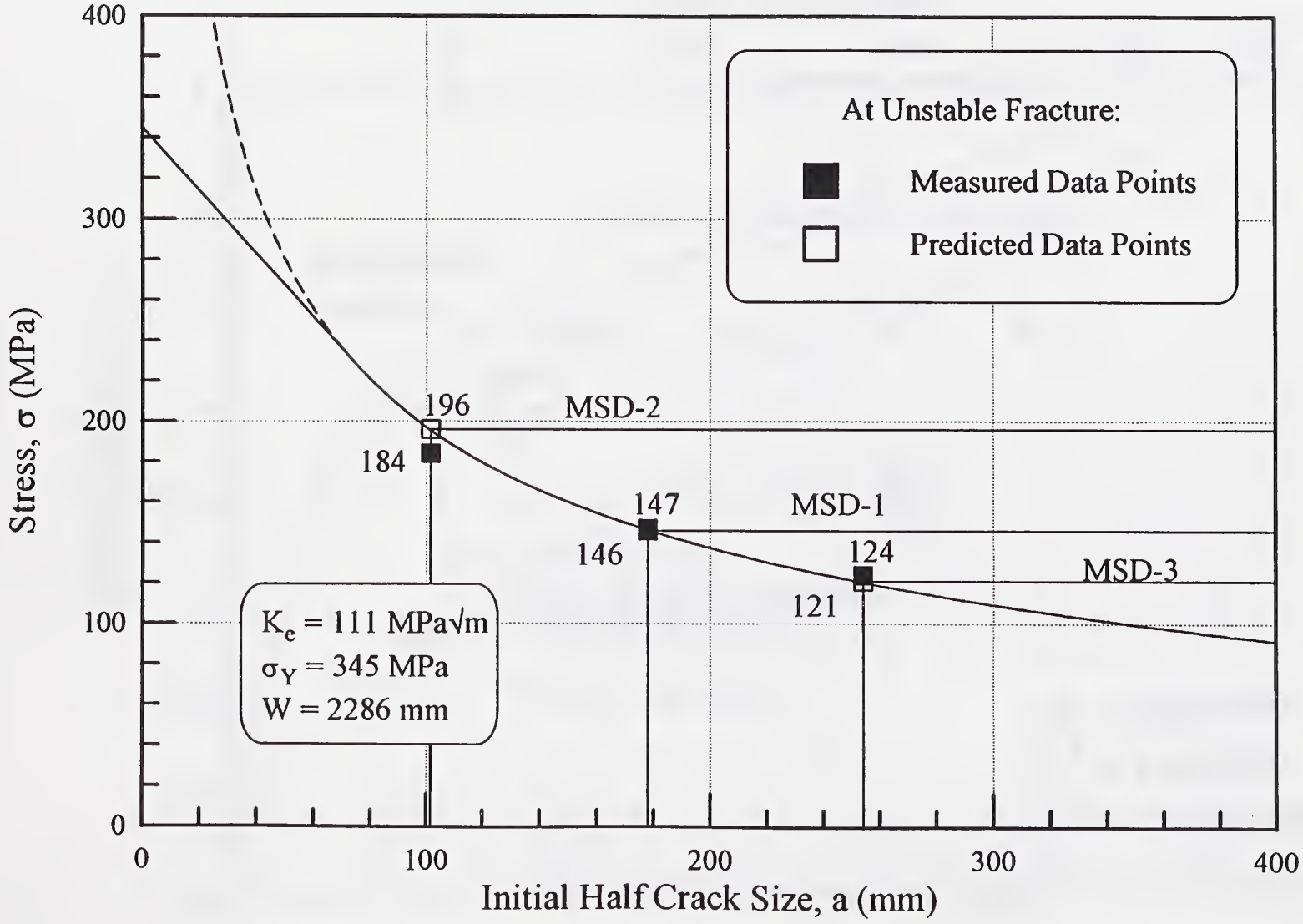

Figure 9. Residual strength diagram for tests MSD-1, 2, and 3, with measured data points and predicted fracture paths

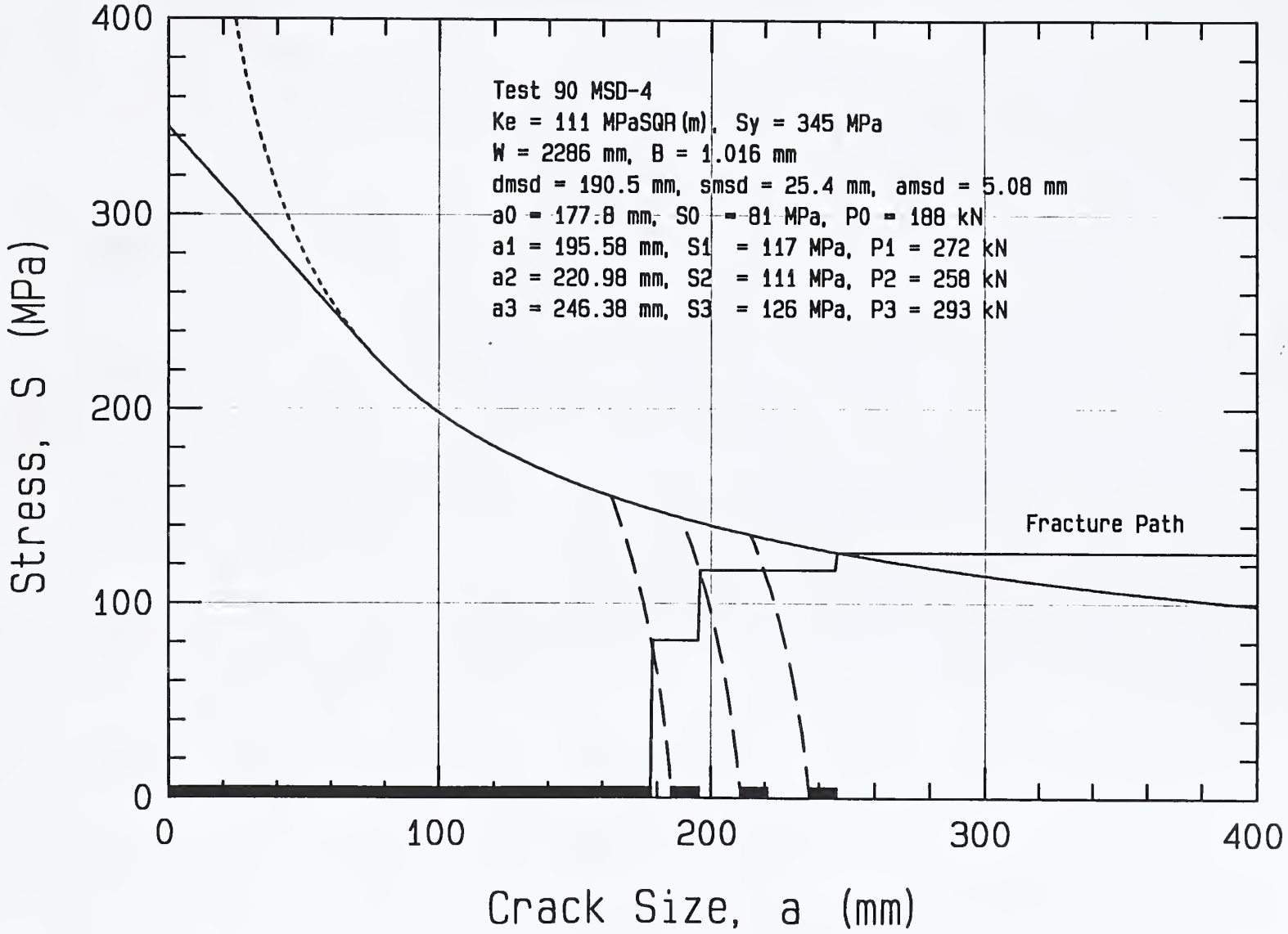

Figure 10. Residual strength diagram for test MSD-4, with plastic zone criteria and predicted fracture path

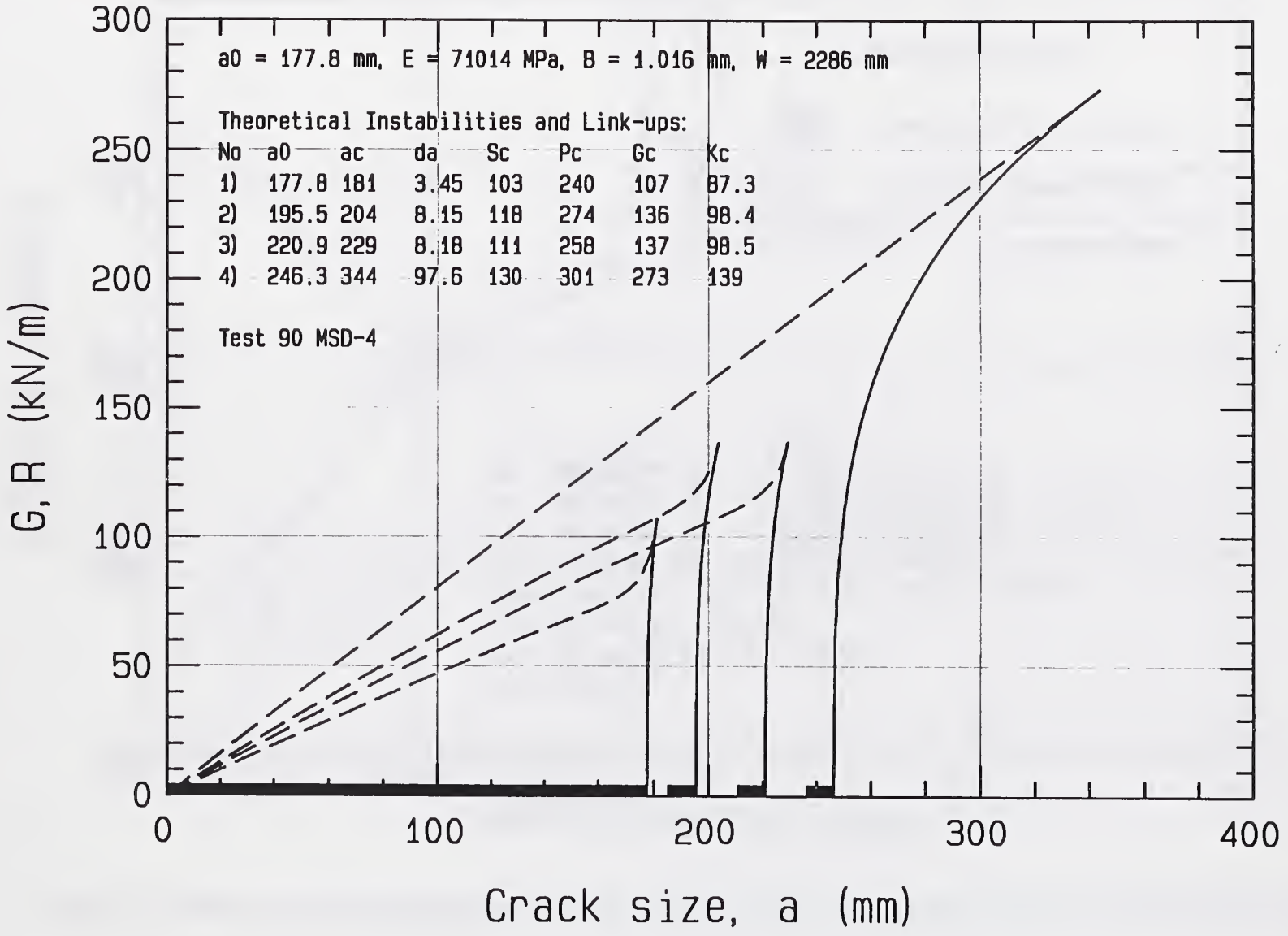

Figure 11. Stability diagram for test 90 MSD-4